Solar Energy Materials & Solar Cells 241 (2022) 111725

Contents lists available at ScienceDirect

Solar Energy Materials and Solar Cells

journal homepage: www.elsevier.com/locate/solmat

Improving the performance of GaInP solar cells through rapid thermal annealing and delta doping

Yukun Sun [a,b,c], Brian D. Li [b,c], Ryan D. Hool [c,d], Shizhao Fan [b,c], Mijung Kim [b,c], Minjoo Larry Lee [b,c,*]

[a] Department of Electrical Engineering, Yale University, New Haven, CT, 06520, USA
[b] Department of Electrical and Computer Engineering, University of Illinois Urbana-Champaign, Urbana, IL, 61801, USA
[c] Nick Holonyak, Jr. Micro and Nanotechnology Laboratory, University of Illinois Urbana-Champaign, Urbana, IL, 61801, USA
[d] Department of Materials Science and Engineering, University of Illinois Urbana-Champaign, Urbana, IL, 61801, USA

ABSTRACT

We show that the effect of rapid thermal annealing (RTA) on carrier lifetime in GaInP grown by molecular beam epitaxy depends strongly on both doping type and density, and that these disparities must be accounted for to realize high-performance GaInP solar cells. Although the photoluminescence intensity and lifetime of lightly doped p- and n-GaInP improved greatly with RTA, heavily doped n^+-GaInP showed sharp degradation upon RTA, preventing the realization of GaInP front-junction solar cells with low emitter sheet resistance. Since a low series resistance is important to achieve high fill factor (FF), we designed a front-junction cell utilizing a thin, lightly doped n-type emitter with delta doping to enhance conductivity, attaining an open-circuit voltage (V_{OC}) of 1.40 V and FF of 86%. We then designed rear-heterojunction solar cells to further leverage the relatively long lifetime of lightly n-doped GaInP (~19 ns). With the help of delta doping in the n-AlInP window to improve surface passivation, we attained a V_{OC} of 1.42 V, similar to cells grown by metal-organic vapor phase epitaxy.

1. Introduction

$Ga_{0.51}In_{0.49}P$ (hereafter GaInP) is the preferred top cell absorber material for high-efficiency multi-junction solar cells (MJSCs) with 2–4 junctions due to its wide bandgap energy (E_g) of ~1.8–1.9 eV [1–5]. In 2-terminal MJSCs where current is matched across all subcells, the GaInP junction yields the highest operating voltage and hence highest output power [2,6]. GaInP solar cells have been demonstrated by metal-organic vapor phase epitaxy (MOVPE) in both front- and rear-junction designs, and with the benefit of strong photon recycling, such cells have achieved $V_{OC} > 1.4$ V and bandgap-voltage offset ($W_{OC} = E_g/q - V_{OC}$) < 400 mV [7–10]. In contrast, the performance of GaInP solar cells grown by molecular beam epitaxy (MBE) has been inferior to those by MOVPE, with a best reported W_{OC} of 505 mV for a front-junction (FJ) cell design without strong photon recycling (i.e. on a GaAs substrate) [11,12]. Furthermore, no rear-heterojunction (RHJ) GaInP cells have been reported by MBE. W_{OC} values of 400–440 mV have been reported for MOVPE-grown FJ cells on absorbing substrates [7,13], while most MBE-grown GaInP cells exhibit $W_{OC} = 500$–600 mV [14,15], attributed to MBE's lower growth temperature (~450–500 °C for MBE vs. ~600–700 °C for MOVPE) and higher defect density [16–18].

Conventional FJ GaInP solar cells employ a thin (i.e. ≤ 100 nm), heavily doped *n*-type emitter, with an equilibrium electron concentration $n_o \geq 1 \times 10^{18}$ cm^{-3} to minimize emitter sheet resistance (R_{sheet}) while maximizing current collection [19]; a low overall series resistance is necessary to attain high fill factor (FF) [20]. Increasing the emitter doping further can help to reduce R_{sheet} [21], but the minority hole diffusion length (L_p) is unavoidably degraded [19,22]. The emitter thickness must be less than L_p to ensure that photo-generated minority holes can diffuse to the space charge region and be collected. A relatively thick emitter (100–200 nm) can help to meet the need for low R_{sheet} (e.g. < 1000 Ω/sq) for space and CPV applications [7,9,19], at the potential cost of reduced collection efficiency at short wavelengths.

RHJ cells grown by MOVPE with a thick, lightly doped n-GaInP absorber and thin p-type AlGaInP back surface field (BSF) were recently demonstrated to have better W_{OC} and external radiative efficiency than conventional FJ cells [7,9]. The wider bandgap energy of the p-type BSF appears to reduce Shockley-Read-Hall (SRH) recombination in the space charge region (SCR), leading to lower dark current J_{02} and improved open-circuit voltage (V_{OC}) [7,19]. The RHJ design mitigates the R_{sheet} dilemma through the use of a thick emitter while relying on long minority hole lifetimes in order for the hole diffusion length (L_p) to be comparable to or longer than the absorber thickness, typically 0.5–1 μm

* Corresponding author. Department of Electrical and Computer Engineering, University of Illinois Urbana-Champaign, Urbana, IL, 61801, USA.
E-mail address: mllee@illinois.edu (M.L. Lee).

https://doi.org/10.1016/j.solmat.2022.111725
Received 24 August 2021; Received in revised form 10 March 2022; Accepted 21 March 2022
Available online 19 April 2022
0927-0248/

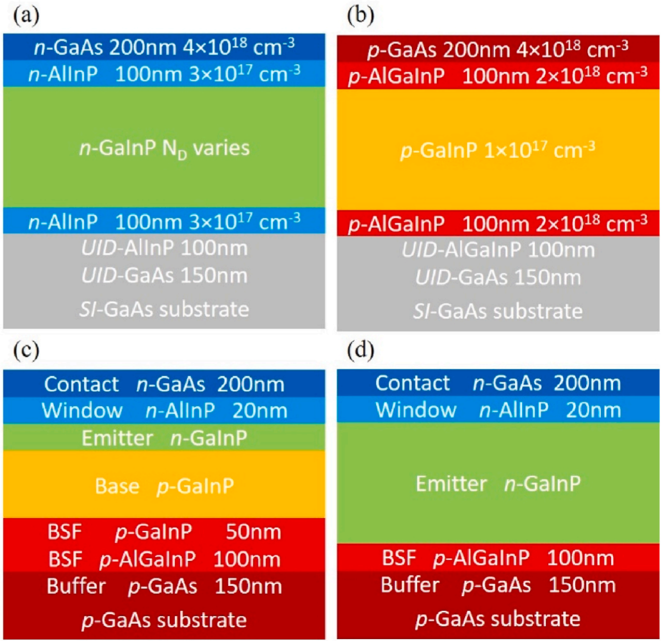

Fig. 1. Layer schematics of (a) n-GaInP DH, (b) p-GaInP DH, (c) GaInP FJ solar cells, and (d) GaInP RHJ solar cells.

[7]. The low hole mobilities in GaInP [23–25] (~18–140 cm^2/Vs) combined with the placement of the SCR at the rear of the device make carrier collection challenging for GaInP RHJ cells [19], demanding low trap density to minimize SRH recombination. In contrast, FJ solar cells can attain high J_{sc} values despite low lifetime through the use of a thin (e.g. ≤ 100 nm) emitter and wide SCR [7,19] (e.g. ≥ 300 nm) while taking advantage of the relatively high electron mobilities in GaInP (~500–2000 cm^2/Vs) [24]. Another challenge that can arise in RHJ cells is insufficient front-side passivation due to Fermi-level pinning in the window layer [26]; undesired band-bending in the absorber region is more prominent in RHJs compared to FJs due to the use of lighter doping in the n-type absorber of RHJ cells.

The high W_{OC} values of MBE-grown GaInP solar cells [11,12] are thought to result from a wide variety of traps, including P-vacancies [27–30], O-related defects [27,29,31–33], and DX centers [29,30, 34–37]. We previously showed that RTA significantly improves MBE-grown FJ 2.0 eV AlGaInP solar cells, enabling efficiencies similar to the best such devices grown by MOVPE [38,39]. The dependence of point defect formation energies on Fermi level position in (Al)GaInP [33, 40] suggests that n- and p-GaInP may respond differently to RTA. Therefore, double heterostructures (DHs) are a simpler system to understand RTA improvement in n- and p-type GaInP individually, allowing the measurement of minority carrier lifetime and the separation of bulk lifetime and surface recombination velocity using time-resolved photoluminescence (TRPL) [41].

In this work, we present a systematic study on the effects of doping and RTA conditions on n- and p-GaInP DHs, finding a long bulk lifetime of ~19 ns in lightly doped n-GaInP with $n_o = 1 \times 10^{17}$ cm^{-3} after RTA. In contrast, the TRPL lifetime of heavily doped n^+-GaInP ($n_o = 2 \times 10^{18}$ cm^{-3}) degrades sharply with RTA. For the case of lightly doped p-GaInP DHs (equilibrium hole concentration, $p_o = 1 \times 10^{17}$ cm^{-3}), bulk lifetime improves with RTA but only rises to 4.3 ns. We go on to describe GaInP FJ solar cells where lightly doped n-GaInP provides a high-quality emitter, while Si delta doping (δ-doping) helps to maintain low emitter R_{sheet}. Such cells reached $V_{OC} = 1.40$ V ($W_{OC} = 493$ mV), which is the best reported value for MBE-grown GaInP; all cells in this work remain on their absorbing GaAs substrates, precluding significant V_{OC} benefits from photon recycling [7,42]. Finally, we present MBE-grown

Table 1
GaInP solar cell design variations and RTA conditions.

Sample	Emitter	Base	δ-doping	RTA
FJ 1	50 nm 2 × 10^{18} cm^{-3}	1500 nm 1 × 10^{17} cm^{-3}	None	1000 °C 1s
FJ 2	70 nm 1 × 10^{18} cm^{-3}	690 nm 1 × 10^{17} cm^{-3}	None	1000 °C 1s
FJ 3	70 nm × 10^{17} cm^{-3}	690 nm 1 × 10^{17} cm^{-3}	4 × 0.005 ML in top 25 nm of emitter	1000 °C 1s
FJ 4	70 nm 1 × 10^{17} cm^{-3}	690 nm 1 × 10^{17} cm^{-3}	4 × 0.010 ML in top 25 nm of emitter	1000 °C 1s
RHJ1	810 nm 1 × 10^{17} cm^{-3}	100 nm 1 × 10^{17} cm^{-3}	None	900 °C 10 s
RHJ2	810 nm 1 × 10^{17} cm^{-3}	100 nm 1 × 10^{17} cm^{-3}	4 × 0.010 ML in window	900 °C 10 s

GaInP RHJ cells that attain $V_{OC} = 1.42$ V ($W_{OC} = 442$ mV) by taking advantage of the reduced non-radiative recombination in lightly doped n-GaInP and improved surface passivation from a δ-doped window. Through consideration of the effects of doping type, concentration, and RTA, we demonstrate that the performance of MBE-grown GaInP cells can approach the best results shown by MOVPE.

2. Experiments

All samples were grown in a Veeco Mod Gen II solid-source MBE system. For DHs, n-type $Al_{0.52}In_{0.48}P$ ($E_g = 2.3$ eV, hereafter AlInP) and p-type $Al_{0.24}Ga_{0.28}In_{0.48}P$ ($E_g = 2.2$ eV, hereafter AlGaInP) were used as cladding layers to mimic the passivation of the window and BSF layers in GaInP solar cells, respectively [layer structures shown in Fig. 1 (a) and (b)]; all layers were grown at a substrate temperature of 460 °C at 0.5 μm/h and doped by Si or Be for n- or p-type doping. We calibrated each layer's composition with high-resolution x-ray diffraction and/or photoluminescence (PL) and carrier concentration with Hall effect measurements. 500 nm was used as the baseline GaInP absorber/emitter thickness in the DHs, and additional DHs with GaInP thickness of 250 and 1000 nm were grown for the extraction of bulk lifetime and surface recombination velocity.

The structure of GaInP FJ solar cells is shown in Fig. 1(c) and includes: a 150 nm p-GaAs buffer ($p_o = 5 \times 10^{18}$ cm^{-3}), 100 nm p-AlGaInP BSF ($p_o = 2 \times 10^{18}$ cm^{-3}), 50 nm p-GaInP BSF (p_o graded from 2×10^{18} to 1×10^{17} cm^{-3}), 690 nm p-GaInP base ($p_o = 1 \times 10^{17}$ cm^{-3}), 70 nm n-GaInP emitter (n_o varies), 20 nm n-AlInP window ($n_o \sim 3 \times 10^{17}$ cm^{-3}), and 200 nm n-GaAs contact ($n_o = 1.2 \times 10^{19}$ cm^{-3}). For GaInP RHJ solar cells (Fig. 1(d)), the p-GaInP layer was eliminated while the thickness of the n-GaInP absorber was set to 810 nm to maintain the same amount of light absorption as the FJ cells; p_o of the p-AlGaInP BSF was also reduced to 1×10^{17} cm^{-3}. The design variations of FJ and RHJ solar cells explored in this work are listed in Table 1 δ-doping was performed by depositing Si atoms during growth pauses under group V overpressure and is given in terms of fraction of a monolayer (ML), where the surface atomic density is 6.26×10^{14} cm^{-2}. The δ-doping dose time was typically 30–60 s and was calculated based on bulk doping calibrations. After growth, DH and solar cell samples were RTA'd at 700–1000 °C for 1–10 s in N_2 ambient while covered by GaAs wafers to prevent As desorption at high temperatures; the RTA conditions for the different solar cell samples are listed in Table 1. A slight increase in E_g (~30 meV) was noted after RTA for the cells studied in this work, which could result from slight changes in the degree of CuPt ordering or removal of defect states [18,43]. Solar cells with area of 1–10 mm^2 were fabricated using standard photolithography and wet-etching methods, and e-beam deposition was used for front and back metal contacts; no anti-reflection coatings were applied to solar cells discussed in this work.

A 532 nm continuous wave laser and Ocean Optics spectrometer were used for steady-state photoluminescence (SSPL), while the 532 nm line of a pulsed super-continuum laser (5.6 MHz repetition rate) and a single photon detection module (ID Quantique, model No. id 100-20)

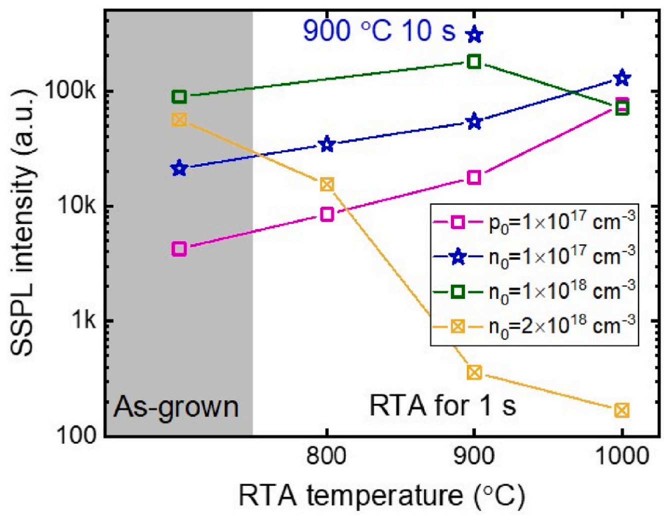

Fig. 2. SSPL intensity of 0.5 μm GaInP DHs after RTA at 800, 900, and 1000 °C for 1 s, showing large enhancements in all cases except n^+-GaInP (yellow), which degrades strongly. The brightest n-GaInP sample investigated in this work was RTA'd at 900 °C for 10 s and is included on this plot for reference. (For interpretation of the references to colour in this figure legend, the reader is referred to the Web version of this article.)

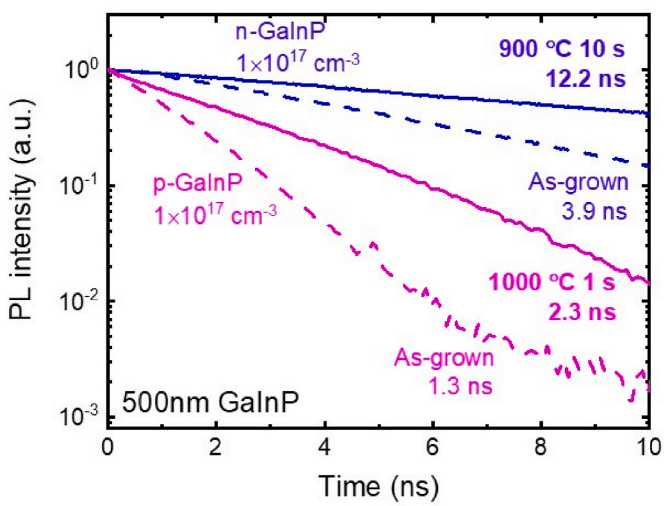

Fig. 3. TRPL decay curves for lightly doped n- and p-GaInP DHs with $n_o = p_o = 1 \times 10^{17}$ cm^{-3}. Lifetime increases strongly with RTA for both, especially for n-type (blue solid). (For interpretation of the references to colour in this figure legend, the reader is referred to the Web version of this article.)

were used for TRPL. Solar cells were fabricated as described in our previous work [14,16]. External quantum efficiency (EQE) and reflectance (R) were measured in a PV Measurements QEX7 system to calculate internal quantum efficiency [IQE = EQE/(1-R)]. Lighted current-voltage characteristics (LIV) of solar cells were measured under approximate AM1.5G conditions using an ABET 10500 solar simulator to determine V_{OC}, short-circuit current density (J_{SC}), FF, and efficiency (η). A Mightex blue LED was used as a light source for Suns-V_{OC} measurement, and dark current parameters J_{01} and J_{02}, corresponding to ideality factors n = 1 and 2, were extracted from Suns-V_{OC} results using a MATLAB program.

3. Results and discussion

3.1. PL study on RTA'd GaInP DHs

Fig. 2 shows that RTA improved the SSPL intensity of all DHs investigated here, except for the n^+-GaInP sample (Fig. 2, yellow). p-GaInP DHs (Fig. 2, magenta) showed nearly monotonic improvements in intensity as a function of increasing RTA temperature. In contrast, the dramatic decrease in SSPL intensity with RTA for the n^+-GaInP DH with $n_o = 2 \times 10^{18}$ cm^{-3} indicates that high temperature steps should be avoided for such heavily n-doped material. n-GaInP with $n_o = 1 \times 10^{18}$ cm^{-3} was far more stable with respect to RTA, though a slight degradation in SSPL occurred after RTA at 1000 °C (Fig. 2, green). Further decreasing n_o to 1×10^{17} cm^{-3} allowed n-GaInP to improve with RTA in a manner similar to p-GaInP, though with higher intensity. The strongest SSPL intensity among all RTA'd GaInP DHs was achieved in n-GaInP with $n_o = 1 \times 10^{17}$ cm^{-3} after a 900 °C 10 s RTA.

TRPL shows that the increase in SSPL intensity for p-GaInP was also accompanied by an increase in carrier lifetime (Fig. 3). Starting from 1.29 ns, the TRPL lifetime (τ_{TRPL}) of p-GaInP DH was improved by 1.8 × to 2.33 ns after RTA at 1000 °C for 1 s (Fig. 3). A bulk lifetime τ_{bulk} of 4.30 ns was extracted from DHs with different thickness (250, 500, and 1000 nm) RTA'd under the same condition (1000 °C for 1 s), approaching previous reports on annealed p-GaInP grown by MBE [44]. Considering that the radiative lifetime τ_{rad} of p-GaInP with $p_o = 1 \times 10^{17}$ cm^{-3} is ~50 ns [45] and that MOVPE-grown p-GaInP DHs with $\tau_{TRPL} = 29$ ns have been reported [45], it is evident that the MBE-grown

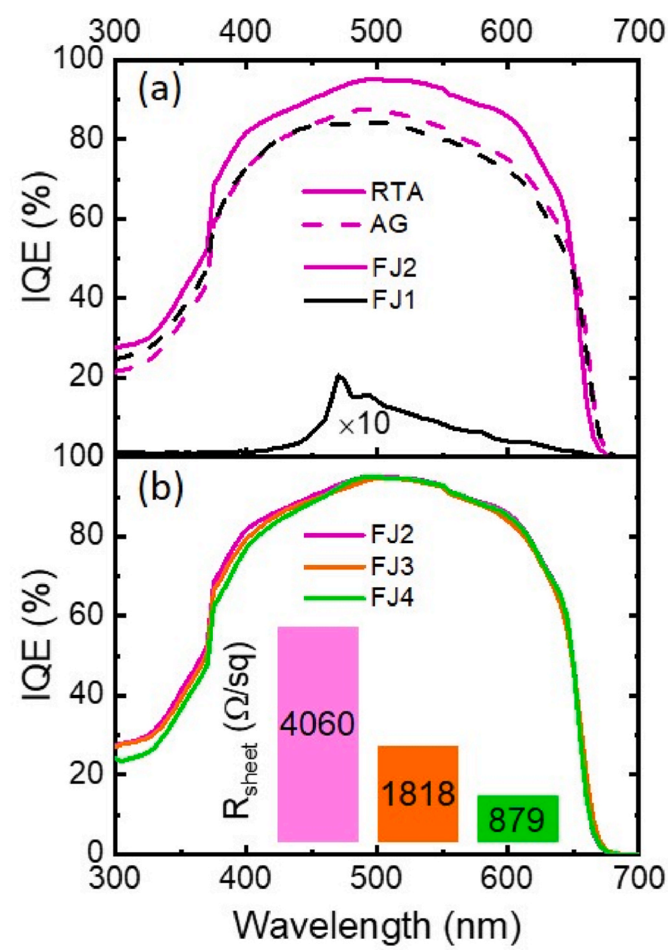

Fig. 4. (a) IQE comparison of as-grown (AG) and RTA'd GaInP FJ cells showing degraded IQE of GaInP FJ with 2×10^{18} cm^{-3} emitter doping, and (b) IQE comparison of bulk- and δ-doped GaInP FJ cells with varying δ doses.

Table 2
Figures of merit of GaInP FJ solar cells (bold for after RTA).

	Emitter doping (cm^{-3})	E_g (eV)	V_{OC} (V)	W_{OC} (mV)	J_{SC} (mA/cm^2)	FF (%)	Efficiency (%)
FJ 1	2×10^{18}	1.864	1.287	576	10.36	79.00	10.53
		\	**0.439**	\	\	**57.07**	\
FJ 2	1×10^{18}	1.862	1.304	558	9.08	82.37	9.75
		1.891	**1.392**	**499**	**10.57**	**84.10**	**12.37**
FJ 3	1×10^{17}	1.867	1.311	556	8.84	82.92	9.61
	4 × 0.005 ML	**1.894**	**1.401**	**493**	**10.36**	**86.27**	**12.52**
FJ 4	1×10^{17}	1.855	1.301	555	8.66	82.39	9.28
	4 × 0.01 ML	**1.882**	**1.388**	**494**	**9.83**	**86.30**	**11.77**

material is limited by SRH recombination. The mechanism of RTA improvement remains unclear due to the lack of deep level transient spectroscopy (DLTS) studies on Be-doped GaInP, but it was shown that the signal from O-related defects was suppressed by RTA in the case of p-AlGaInP [40].

Lightly doped n-GaInP DHs attain considerably longer τ_{TRPL} than p-GaInP, demonstrating the promise of MBE-grown GaInP RHJ cells (Fig. 3). As grown, the τ_{TRPL} of 3.85 ns for n-GaInP already surpasses that of RTA'd p-GaInP (Fig. 3, blue dashed), and the τ_{TRPL} of 12.2 ns after RTA at 900 °C 10 s surpasses any previous report for MBE-grown phosphide material [44,46]. A τ_{bulk} of 19.0 ns was extracted from thickness studies of samples RTA'd at 900 °C for 10 s, and an SRH recombination lifetime of 30.6 ns was estimated with the assumption of $\tau_{rad} = 50$ ns [46,47]. For n-GaInP with $n_o = 1 \times 10^{18}$ cm^{-3}, a τ_{TRPL} of 6.1 ns lifetime was measured after RTA at 900 °C 10 s (not shown), which is slightly longer than the estimated τ_{rad} of ~5 ns and indicative of possible photon recycling effects [48]. Previous studies provide clues though no definitive answer as to why the RTA improvement in n-GaInP is stronger than in p-GaInP. For example, O-related defects were discovered in n-GaInP [29,31–33], and re-arrangement of O-related defects was proposed as a mechanism for changes in the DLTS spectra after RTA [27]. Furthermore, the DLTS signals from P vacancies, their defect complexes with O, and DX-type centers were all shown to be suppressed in n-GaInP by RTA [29,34,35,30]. Finally we speculate that the precipitous SSPL degradation with RTA observed in the n^+-GaInP DH could be related to a doping-induced decrease in formation energy for an as-yet unidentified native trap state; heavy n-type doping pushes the Fermi level into the conduction band [49,50], and the thermal energy provided during RTA could accelerate the formation of native defects, causing rapid degradation.

3.2. GaInP FJ solar cells

Taking advantage of our new understanding of the effects of RTA on GaInP, we reduced the emitter doping of our GaInP FJ solar cells from 2×10^{18} cm^{-3} (FJ1) to 1×10^{18} cm^{-3} (FJ2). As shown in Table 1, the emitter thickness was increased from 50 nm in FJ1 to 70 nm in FJ2 in an attempt to reduce R_{sheet}. Although FJ1 and FJ2 showed similar IQE before RTA (Fig. 4(a), dashed), a 1000 °C 1s RTA improved the IQE of GaInP FJ2 across all wavelengths (Fig. 4(a), magenta), consistent with the improved PL described above. In stark contrast, the same RTA treatment on FJ1 decimated IQE at all wavelengths (Fig. 4(a), black solid) with a peak value of ~2%, consistent with the sharp PL degradation of RTA'd 2×10^{18} cm^{-3} n^+-GaInP DHs. A peak IQE value of 95.2% was achieved in FJ2, though some IQE loss is observed close to the band-edge due to low absorber thickness and the lack of a back reflector [7]. While the reduced emitter doping of FJ2 enabled high IQE and $V_{OC} = 1.39$ V after RTA, Hall effect measurements showed a high R_{sheet} of 4060 Ω/sq, which is undesirable for concentrator applications.

We next grew FJ cells with a light emitter doping of $N_D = 1 \times 10^{17}$ cm^{-3} while adding 4 × Si δ-doping spikes in the top 25 nm to explore the possibility of realizing high material quality while maintaining low R_{sheet}. Hall measurements showed that δ-doping was successful in reducing R_{sheet} to 1818 and 879 Ω/sq in FJ3 (4 × 0.005 ML δ spikes) and FJ4 (4 × 0.01 ML δ spikes), respectively, despite band simulations showing a very thin (~25 nm) conducting channel with most of the emitter depleted. The emitter sheet carrier density, as measured by Hall Effect, increased with additional Si dose from 2.4×10^{12} cm^{-2} (FJ2) to 7.3×10^{12} cm^{-2} (FJ3) and 1.6×10^{13} cm^{-2} (FJ4), suggesting efficient dopant activation within the δ spikes. IQE of GaInP FJs was not strongly affected by δ-doping (Fig. 4(b)), showing its usefulness in achieving low

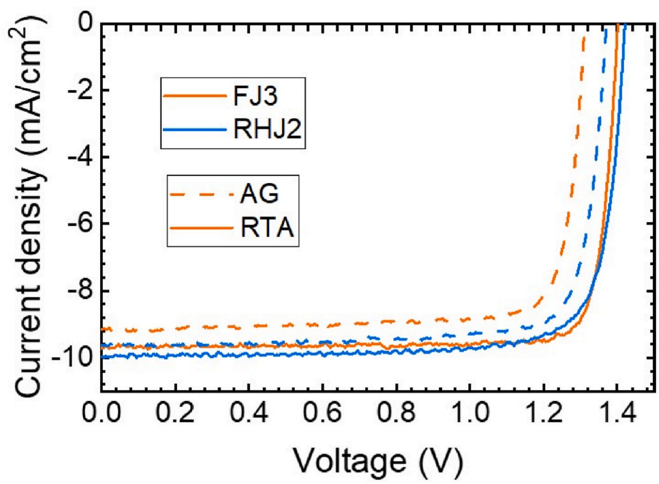

Fig. 5. LIV characteristics of FJ3 (orange) and RHJ2 (blue) solar cells before (dashed) and after RTA (solid). (For interpretation of the references to colour in this figure legend, the reader is referred to the Web version of this article.)

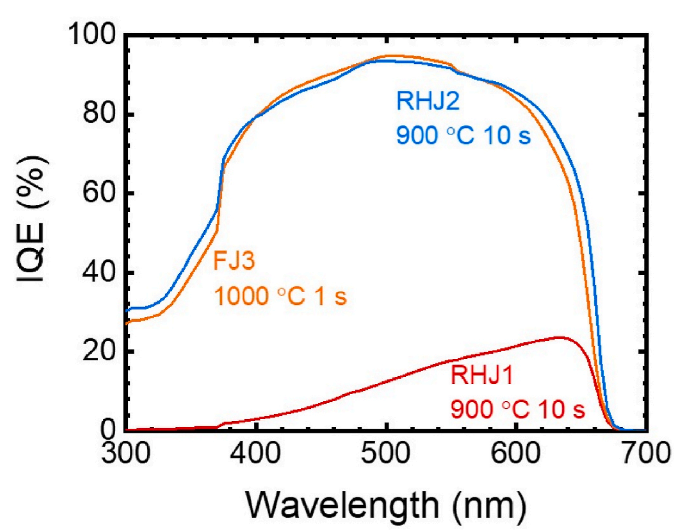

Fig. 6. IQE comparison of FJ3 (orange), RHJ w/δ-doping (blue), and RHJ w/o δ-doping (red) showing the improvement of RHJ by the addition of 4 × 0.01 ML δ-doping in the window layer. (For interpretation of the references to colour in this figure legend, the reader is referred to the Web version of this article.)

Table 3
Figures of merit of GaInP RHJ solar cells.

Sample	Window layer	E_g (eV)	V_{OC} (V)	W_{OC} (mV)	J_{SC} (mA/cm^2)	FF (%)	Efficiency (%)
RHJ1	No δ-doping	1.843	1.097	746	0.78	58.48	0.50
		1.849	**1.191**	**658**	**1.92**	**68.51**	**1.57**
RHJ2	4 × 0.01 ML	1.861	1.370	491	9.61	81.88	10.78
		1.862	**1.420**	**442**	**10.17**	**84.70**	**12.23**

R_{sheet} without diffusion length degradation.

Our approach of using light bulk doping with δ-doping spikes was further validated by the V_{OC} of 1.401 V from FJ3 after 1000 °C 1 s RTA (Table 2 and Fig. 5), which is better than any previously reported MBE-grown FJ GaInP cell [11,12,15]. The increased minority carrier diffusion length after RTA suppressed field-assisted carrier collection [38] and boosted FF to >86% (Table 2). Suns-V_{OC} measurements show that J_{01} and J_{02} values of FJ3 decreased by 26 × and 4 × , respectively after RTA, indicating strong minority carrier lifetime improvement in both the quasi-neutral and space-charge regions. Taken together, these results show that RTA can be used to improve the quality of both p- and n-GaInP with light-to-moderate doping and that δ-doping can reduce R_{sheet} without thermally induced degradation. Future work is needed to better understand why n^+-GaInP with $N_D = 2 \times 10^{18}$ cm^{-3} degrades strongly with RTA, while δ-doped n-GaInP with equivalent or greater sheet carrier concentration does not.

3.3. GaInP RHJ solar cells

We next sought to take advantage of the strong RTA improvements in lightly doped n-GaInP in RHJ cells. However, the first iteration (RHJ1) suffered from poor IQE (Fig. 6, red) and very low V_{OC} (1.191 V, Table 3). Si activation in MBE-grown n-AlInP is typically <50% [51], which can lead to undesirable band-bending extending deep into the lightly doped absorber. Increasing the window layer thickness can mitigate the band-bending at the cost of parasitic optical absorption in the n-AlInP [24]. As an alternative approach, we added 4 × 0.01 ML δ-doping spikes in the window (RHJ2) to flatten the bands while maintaining a low window layer thickness of 20 nm. The sheet carrier concentration and R_{sheet} of n-type layers in RHJ2 improved to 8.65×10^{12} cm^{-2} and 808 Ω/sq, respectively, compared to 5.40×10^{12} cm^{-2} and 1295 Ω/sq in RHJ1. The improvement in R_{sheet} gained by δ-doping is similar to what would be achieved in a >100 nm n-AlInP window with only bulk doping, but without added parasitic optical absorption.

The addition of δ-doping to the window transformed the performance of our RHJ cells (red vs blue curves in Fig. 6). RHJ2 showed comparable IQE to FJ3 after RTA (blue and orange curves in Fig. 6) despite the much lower diffusivity of holes compared to electrons in GaInP, while demonstrating the effectiveness of window δ-doping in preventing surface-induced depletion from penetrating into the absorber. Moreover, RHJ2 showed an as-grown W_{OC} of 491 mV (Table 3), which is already better than the lowest FJ W_{OC} after RTA (Table 2). The W_{OC} of 442 mV for RHJ2 after RTA closely approaches the W_{OC} for MOVPE-grown, on-substrate GaInP RHJ cells [7]. Based on Suns-V_{OC} measurement and reciprocity relations in solar cells [52,53], an external radiative efficiency of ~0.1% was estimated; in comparison, ERE values of 0.002% and 0.022% were estimated for FJ3 before and after RTA, respectively. FF of our current-best RHJ cells is still limited by J_{02}, motivating future work to reduce recombination in the SCR [7,19].

4. Conclusions

Understanding the combined effects of dopant species, concentration, and RTA on τ_{TRPL} in MBE-grown GaInP simultaneously drove us to redesign our FJ cells and enabled us to demonstrate high-performance RHJ cells. Since the longest lifetimes in this work were observed in lightly doped n-GaInP, we implemented δ-doping in distinct ways for both FJ and RHJ cells to ensure favorable electrostatics for each cell type. In FJ cells, δ-doping in the emitter enables a unique combination of low R_{sheet} and high IQE at short wavelengths, while in RHJ cells, δ-doping in the window appears to prevent surface Fermi level pinning, enabling both high V_{OC} and IQE.

CRediT authorship contribution statement

Yukun Sun: Conceptualization, Investigation, Methodology, Writing – original draft. **Brian D. Li:** Investigation, Writing – review & editing. **Ryan D. Hool:** Writing – review & editing, Investigation. **Shizhao Fan:** Investigation. **Mijung Kim:** Investigation. **Minjoo Larry Lee:** Conceptualization, Funding acquisition, Project administration, Writing – review & editing.

Declaration of competing interest

The authors declare that they have no known competing financial interests or personal relationships that could have appeared to influence the work reported in this paper.

Acknowledgment

We gratefully acknowledge funding from NSF (Grants No. 1736181 and 1810265). R.D.H. and B.D.L were supported by NASA Space Technology Research Fellowships (Grants No. 80NSSC18K1171 and 80NSSC19K1174). This research was carried out in part in the Materials Research Laboratory Central Research Facilities, University of Illinois Urbana-Champaign.

Appendix A. Supplementary data

Supplementary data to this article can be found online at https://doi.org/10.1016/j.solmat.2022.111725.

References

[1] M.A. Green, E.D. Dunlop, J. Hohl-Ebinger, M. Yoshita, N. Kopidakis, X. Hao, Prog. Photovoltaics Res. Appl. 28 (2020) 629.
[2] N.H. Karam, S. Mesropian, C.M. Fetzer, D.C. Law, K.M. Edmondson, D. Larrabee, D. Bhusari, X.-Q. Liu, W. Hong, A. Boca, R.R. King, 24th Eur. Photovolt. Sol. Energy Conf. 21-25 Sept. 2009 Hambg. Ger. 55 (2009).
[3] J.F. Geisz, S. Kurtz, M.W. Wanlass, J.S. Ward, A. Duda, D.J. Friedman, J.M. Olson, W.E. McMahon, T.E. Moriarty, J.T. Kiehl, Appl. Phys. Lett. 91 (2007), 023502.
[4] K. Sasaki, T. Agui, K. Nakaido, N. Takahashi, R. Onitsuka, T. Takamoto, AIP Conf. Proc. 1556 (2013) 22.
[5] M. Feifel, D. Lackner, J. Ohlmann, J. Benick, M. Hermle, F. Dimroth, Sol. RRL 3 (2019) 1900313.
[6] D.J. Aiken, A.B. Cornfeld, M.A. Stan, P.R. Sharps, 2006 IEEE 4th World Conf. Photovolt. Energy Conf (2006) 838–841.
[7] J.F. Geisz, M.A. Steiner, I. García, S.R. Kurtz, D.J. Friedman, Appl. Phys. Lett. 103 (2013), 041118.
[8] (ORCID:0000000225947810) M.A. Green, E.D. Dunlop, D.H. Levi, J. Hohl-Ebinger, M. Yoshita, A.W.Y. Ho-Baillie, Prog. Photovoltaics Res. Appl. 27 (2019).
[9] M. Hinojosa, I. García, I. Rey-Stolle, C. Algora, Sol. Energy Mater. Sol. Cells 205 (2020) 110235.
[10] R.R. King, D. Bhusari, A. Boca, D. Larrabee, X.-Q. Liu, W. Hong, C.M. Fetzer, D. C. Law, N.H. Karam, Prog. Photovoltaics Res. Appl. 19 (2011) 797.
[11] S. Lu, L. Ji, W. He, P. Dai, H. Yang, M. Arimochi, H. Yoshida, S. Uchida, M. Ikeda, Nanoscale Res. Lett. 6 (2011) 576.
[12] P. Dai, S.L. Lu, Y.Q. Zhu, L. Ji, W. He, M. Tan, H. Yang, M. Arimochi, H. Yoshida, S. Uchida, M. Ikeda, J. Cryst. Growth 378 (2013) 604.
[13] M.A. Steiner, R.M. France, J. Buencuerpo, J.F. Geisz, M.P. Nielsen, A. Pusch, W. J. Olavarria, M. Young, N.J. Ekins-Daukes, Adv. Energy Mater. 11 (2021) 2002874.

[14] T. Masuda, S. Tomasulo, J.R. Lang, M.L. Lee, J. Appl. Phys. 117 (2015), 094504.
[15] J.T. Boyer, D.L. Lepkowski, D.J. Chmielewski, T.J. Grassman, Sol. Energy Mater. Sol. Cells 202 (2019) 110133.
[16] J. Faucher, Y. Sun, D. Jung, D. Martin, T. Masuda, M.L. Lee, Appl. Phys. Lett. 109 (2016) 172105.
[17] M. Jalonen, M. Toivonen, P. Savolainen, J. Köngäs, M. Pessa, Appl. Phys. Lett. 71 (1997) 479.
[18] S.F. Yoon, K.W. Mah, H.Q. Zheng, J. Alloys Compd. 280 (1998) 299.
[19] Y. Sun, A. Perna, P. Bermel, IEEE J. Photovolt. 9 (2019) 437.
[20] M.A. Green, Sol. Cell. 7 (1982) 337.
[21] M. Ochoa, E. Barrigón, L. Barrutia, I. García, I. Rey-Stolle, C. Algora, Prog. Photovoltaics Res. Appl. 24 (2016) 1332.
[22] M.A. Steiner, R.M. France, E.E. Perl, D.J. Friedman, J. Simon, J.F. Geisz, IEEE J. Photovolt. 1 (2019).
[23] M. Ikeda, K. Kaneko, J. Appl. Phys. 66 (1989) 5285.
[24] T. Shitara, K. Eberl, Appl. Phys. Lett. 65 (1994) 356.
[25] R.R. King, J.H. Ermer, D.E. Joslin, M. Haddad, J.W. Eldredge, N.H. Karam, B. Keyes, R.K. Ahrenkiel, 2nd World Conf. Photovolt. Sol. Energy Convers. (1998) 86–90.
[26] D.L. Lepkowski, J.T. Boyer, D.J. Chmielewski, A.C. Silvaggio, S.A. Ringel, T. J. Grassman, IEEE J. Photovolt. 9 (2019) 1644.
[27] A. Tukiainen, J. Dekker, N. Xiang, M. Pessa, Phys. Scripta T114 (2004) 9.
[28] M. Lueck, M. Gonzalez, Ojin Kwon, C. Andre, S.A. Ringel, Conf. Rec. Thirty-First IEEE Photovolt. Spec. Conf. 2005 (2005) 711–714.
[29] N. Xiang, A. Tukiainen, J. Dekker, J. Likonen, M. Pessa, J. Cryst. Growth 227–228 (2001) 244.
[30] J. Dekker, A. Tukiainen, N. Xiang, S. Orsila, M. Saarinen, M. Toivonen, M. Pessa, N. Tkachenko, H. Lemmetyinen, J. Appl. Phys. 86 (1999) 3709.
[31] A. Knauer, P. Krispin, V.R. Balakrishnan, M. Weyers, J. Cryst. Growth 272 (2004) 627.
[32] W.E. Hoke, P.J. Lemonias, A. Torabi, J. Vac. Sci. Technol. B Microelectron. Nanometer Struct. Process. Meas. Phenom. 16 (1998) 3041.
[33] N. Xiang, A. Tukiainen, M. Pessa, J. Dekker, J. Likonen, J. Mater. Sci. Mater. Electron. 13 (2002) 549.
[34] J.H. Kim, S.J. Jo, J.W. Kim, J.-I. Song, J. Appl. Phys. 89 (2001) 4407.
[35] E.C. Paloura, A. Ginoudi, G. Kiriakidis, A. Christou, Appl. Phys. Lett. 59 (1991) 3127.
[36] S. Nojima, H. Tanaka, H. Asahi, J. Appl. Phys. 59 (1986) 3489.
[37] J. Krynicki, M.A. Zaidi, M. Zazoui, J.C. Bourgoin, M. DiForte-Poisson, C. Brylinski, S.L. Delage, H. Blanck, J. Appl. Phys. 74 (1993) 260.
[38] Y. Sun, S. Fan, J. Faucher, R.D. Hool, B.D. Li, P. Dhingra, M.L. Lee, Sol. Energy Mater. Sol. Cells 219 (2021) 110774.
[39] E.E. Perl, J. Simon, J.F. Geisz, W. Olavarria, M. Young, A. Duda, D.J. Friedman, M. A. Steiner, IEEE J. Photovolt. 6 (2016) 770.
[40] A. Tukiainen, J. Dekker, T. Leinonen, M. Pessa, Mater. Sci. Eng. B 91–92 (2002) 389.
[41] R. Dagan, Y. Rosenwaks, A. Kribus, A.W. Walker, J. Ohlmann, F. Dimroth, Appl. Phys. Lett. 109 (2016) 222106.
[42] M.A. Steiner, J.F. Geisz, I. García, D.J. Friedman, A. Duda, S.R. Kurtz, J. Appl. Phys. 113 (2013) 123109.
[43] S.F. Yoon, K.W. Mah, H.Q. Zheng, P.H. Zhang, J. Cryst. Growth 208 (2000) 197.
[44] N.M. Haegel, T. Christian, C. Scandrett, A.G. Norman, A. Mascarenhas, P. Misra, T. Liu, A. Sukiasyan, E. Pickett, H. Yuen, Appl. Phys. Lett. 105 (2014) 202116.
[45] E.E. Perl, D. Kuciauskas, J. Simon, D.J. Friedman, M.A. Steiner, J. Appl. Phys. 122 (2017) 233102.
[46] R.K. Ahrenkiel, S.P. Ahrenkiel, Theory and Methods of Photovoltaic Material Characterization: Optical and Electrical Measurement Techniques, WORLD SCIENTIFIC, 2019.
[47] C.L. Andre, III-V Semiconductors on SiGe Substrates for Multi-Junction Photovoltaics, The Ohio State University, 2004.
[48] S.M. Sze, K.K. Ng, Physics of Semiconductor Devices, John Wiley & Sons, 2006.
[49] W. Walukiewicz, Phys. B Condens. Matter 302–303 (2001) 123.
[50] W. Walukiewicz, Phys. Rev. B 37 (1988) 4760.
[51] S. Tomasulo, J. Simon, P.J. Simmonds, J. Biagiotti, M.L. Lee, J. Vac. Sci. Technol., B 29 (2011), 03C118.
[52] U. Rau, Phys. Rev. B 76 (2007).
[53] U. Rau, B. Blank, T.C.M. Müller, T. Kirchartz, Phys. Rev. Appl. 7 (2017), 044016.